PNAS RESEARCH ARTICLE | APPLIED PHYSICAL SCIENCES

Quantifying the hydrodynamic contribution to electrical transport in non-Brownian suspensions

Han Lin[a], Madhu V. Majji[b], Noah Cho[a], John R. Zeeman[a], James W. Swan[b,1], and Jeffrey J. Richards[a,2]

Edited by David Weitz, Harvard University, Cambridge, MA; received February 25, 2022; accepted June 4, 2022

Electrical transport in semiconducting and metallic particle suspensions is an enabling feature of emerging grid-scale battery technologies. Although the physics of the transport process plays a key role in these technologies, no universal framework has yet emerged. Here, we examine the important contribution of shear flow to the electrical transport of non-Brownian suspensions. We find that these suspensions exhibit a strong dependence of the transport rate on the particle volume fraction and applied shear rate, which enables the conductivity to be dynamically changed by over 10^7 decades based on the applied shear rate. We combine experiments and simulations to conclude that the transport process relies on a combination of charge and particle diffusion with a rate that can be predicted using a quantitative physical model that incorporates the self-diffusion of the particles.

suspensions | electrical properties | rheology | charge carrier diffusion | Stokesian dynamics

Significance

This work represents a significant advance in the scientific understanding of electronic transport in fluids containing conducting particles. We anticipate that our findings will have a considerable impact on emerging electrical energy storage technologies in which these fluids are found. Our work also has a potential impact on the design of next-generation grid-scale electrochemical storage and water deionization technologies due to the identified physical phenomenon that could impact other fields, including mechano-electric transduction, strain sensing, and neuromorphic computing.

Next-generation electrochemical storage and water deionization technologies demand colloidal fluids that maintain electrical percolation under flow. In these suspensions, metallic and semiconducting nanoparticles, such as carbon black, provide a transient and percolated electrical network, often compared to conductive polymer composites. However, the key distinguishing feature is the potential contribution of particle motion to the transport process. Rheo-electric measurements of such suspensions frequently exhibit an increase in conductivity with increasing shear rate, whose origin has been hypothesized to be shear-induced collisions (1, 2). Kinetic Monte Carlo simulations of flowing slurry suspensions suggest that these dynamic processes account for many features of the system performance. However, there has not yet been direct experimental evidence that these dynamics are present or important in the properties of these suspensions. Despite the extensive experimental work examining the electrical response of carbon under flow in various solvents (3–7) and in the presence of salts (8–10), quantitative accounting for these dynamics in electrical measurements is hampered by the complex microstructural hierarchy that evolves when the suspension is subjected to transient and steady flows (11–13).

To avoid these complexities and chart a pathway toward a quantitative microscopic description, we formulate suspensions containing non-Brownian conducting microspheres. By carefully selecting the properties of the solvent continuous phase, we suppress the effects of Brownian motion, the sedimentation of the particles, and the ability of the particles to aggregate on time scales commensurate with the rheo-electric measurements. Thus, the shear rate dependence of the electrical response in the absence of other contributions is isolated. The electrical properties in shear flow are measured using a custom-built rheo-electric device that can perform transient and steady shear experiments with electrical measurements simultaneously. We show that the electrical conductivity of these suspensions increases instantaneously and reversibly upon flow startup, and the magnitude of the conductivity scales nonlinearly with increasing shear rate and volume fraction. Chrono-amperometry experiments and impedance spectroscopy (IS) are utilized to probe the dynamics of the transport process. We use this experimental insight to propose a scaling law that reveals a single relationship between the electron diffusion and the scaling parameter, linking the volume fraction and shear rate to the conductivity. Finally, we examine the origin of this nonlinearity with IS and show that it arises due to an increase in the dielectric strength of the dipole associated with the short-ranged hopping process. We combine experiments with large-scale Stokesian dynamic simulations coupled with Monte Carlo–based charge transport calculation that provides quantitative agreement with our experimentally determined electrical diffusivity and show that it exceeds the gradient diffusivity of the particles. This is possible because charge displacements along the gradient direction allow transport over dynamic clusters that orient in the compressional direction of shear.

Author affiliations: [a]Department of Chemical & Biological Engineering, Northwestern University, Evanston, IL 60208; and [b]Department of Chemical Engineering, Massachusetts Institute of Technology, Cambridge, MA 02139

Author contributions: H.L. and J.J.R. designed research; H.L., M.V.M., N.C., J.R.Z., and J.J.R. performed research; H.L., M.V.M., N.C., J.R.Z., J.W.S., and J.J.R. analyzed data; and H.L., M.V.M., N.C., J.R.Z., J.W.S., and J.J.R. wrote the paper.

The authors declare no competing interest.

This article is a PNAS Direct Submission.

[1]J.W.S. Deceased November 5, 2021.

[2]To whom correspondence may be addressed. Email: jeffrey.richards@northwestern.edu.

This article contains supporting information online at http://www.pnas.org/lookup/suppl/doi:10.1073/pnas.2203470119/-/DCSupplemental.

Published July 12, 2022.

Results and Discussion

The suspensions were characterized by performing rheology as a function of shear rate ($\dot{\gamma}$) and volume fraction (ϕ). We observed that the suspensions were stable against aggregation for several hours and could be reversibly homogenized. We averaged the viscosity over the last 20 s at each shear rate and calculated the reduced viscosity as (14,15)

$$\eta_r = \eta(\dot{\gamma})/\eta_m \quad [1]$$

using the solvent viscosity $\eta_m = 200 mPa \cdot s$. The resulting reduced viscosity versus shear rate is shown in Fig. 1*A* where ϕ is from 0 to 0.40. The viscosity was averaged over the range of the tested shear rates, as shown in Fig. 1*B* versus ϕ. The experimental viscosities were overlaid with an empirical fit to a modified Krieger-Dougherty equation,

$$\eta_r = \left(1 - \frac{\phi}{\phi_{max}}\right)^{-2}. \quad [2]$$

From this fit, the maximum packing fraction ϕ_{max} is determined to be 0.67, which is close to that found for repulsive-driven glass (16). These results indicate that suspensions are well behaved and non-Brownian.

In this work, the field-dependent measurements of the sheared suspensions exhibit the simple Ohmic behavior, as demonstrated in *SI Appendix*, Fig. S1. To acquire the electrical response of these suspensions, we carried out rheo-electric measurements on a $\phi = 0.35$ suspension. For each shear rate tested, the sample was first presheared at 500 1/s for 30 s, sheared at the desired shear rate for 30 s, and then stopped for 30 s. Throughout the test, the transient current density j, viscosity η, and shear rate $\dot{\gamma}$ were recorded, and three representative shear rate cycles are shown in Fig. 2*A*. We observed j was a strong function of applied shear rate, and the viscosity remained Newtonian. Over repeated cycles, the current returned instantaneously and reproducibly to the same value for any shear rate. Further, during each 30-s period where the shear was arrested, the current density rapidly dropped below the resolution of our source meter, ~100 pA. To test whether the electrical response was sensitive to the flow direction, a shear reversal experiment was performed on the same sample (Fig. 2*B*). The measured current density was unaffected by the shear reversal test at $\dot{\gamma}$=100 1/s, which demonstrated that both current and viscosity are independent of the shear direction. We repeated the protocol described in Fig. 2*A* for other volume fractions (0.25, 0.30, 0.35, 0.40) and shear rates. The steady-state current density j_{ss} that exceeded the resolution of the source meter was averaged over the last 5 s of the acquisition for each shear rate, (Fig. 2*C*). This protocol reveals a strong dependence of j_{ss} on both the volume fraction and the shear rate. The magnitude of j_{ss} was also nonlinear with respect to the shear rate at the highest volume fractions. In our rheo-electric measurements, the electrical field and velocity gradient are parallel (Fig. 2*C*, *Insets*). Thus, it is notable that these measurements were performed using a weak electric field strength, $E_0 \sim 10^1 - 10^2\ V/m$, which was far below that required to induce the structuring of particles observed in electrorheological fluids where the viscosity of the suspension can increase by orders of magnitude for electric fields of 10^6 V/m. We also observe that the viscosity was unchanged by the electric field, indicating the structure of the suspension remains unaffected. Estimates of the Mason number, a dimensionless balance of the viscous to electrostatic forces, given as

$$Mn = \frac{\eta_m \dot{\gamma}}{2\varepsilon_m \beta^2 E_0^2} = 10^{7-11}, \quad [3]$$

confirms that the viscous forces were dominant in our experiments (17).

In addition to the electrical response, a subtle time-dependent current relaxation was visible for some experimental conditions upon shear rate changes. In these cases, the transient electrical response was correlated with a viscous relaxation. However, there were instances when the electrical relaxation occurred in the absence of a transient viscosity. While the origin of the viscous relaxation was likely particle migration (18) or microstructural rearrangement that originates from the finite Van der Waal's force between silver particles, the same effects would not necessarily produce an electrical relaxation. Unfortunately, the protocol described in Fig. 2 did not allow us to probe this systematically. Therefore, we performed chronoamperometry on the suspensions at a constant shear rate. The electrical potential Φ was alternated between 1 and −1 V every 120 s while the viscosity and the electrical current were recorded simultaneously. A representative measurement for $\dot{\gamma} = 100$ 1/s is shown in Fig. 3*A*. For each step change in potential, we observed a constant viscosity and a reproducible transient electrical relaxation. In contrast to the results in Fig. 2, this protocol demonstrated that the transient current occurred independently from microstructural rearrangement, as the viscosity remained constant during the step-change in potential.

These observations are a hallmark of charge carrier diffusion (19), and in our measurements, we found that the rate of relaxation of the transient current was a function of the shear rate. As shown in Fig. 3*B*, the absolute value of current density was averaged for each potential pulse, excluding the first pulse because of the unsteady viscosity. To quantify the current relaxation, we fit our experimental data using

$$\langle |j| \rangle = j_0 e^{-t/\tau} + j_{ss}, \quad [4]$$

where j_{ss} is defined as above, j_0 is the magnitude of the current density after potential reversal, and τ is the characteristic relaxation rate. Fits of the transient electrical response are shown for $\phi = 0.30$ and $\dot{\gamma} = 20 - 100\ 1/s$ in Fig. 3*B* and accurately described the experimental data. Similar measurements were applied to other volume fractions (0.20, 0.25, 0.30, 0.35), and for shear rates where a transient relaxation was present, the fit parameters versus shear rates were summarized in Fig. 3*C*. These measurements confirmed that in general, the relaxation

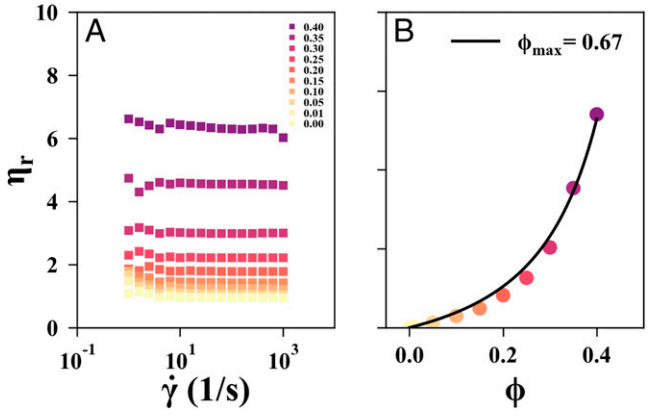

Fig. 1. (*A* and *B*) Reduced viscosity η_r versus $\dot{\gamma}$ as a function of ϕ (0 to 0.40) (*A*) and the averaged reduced viscosity η_r versus ϕ, solid line: fit to the modified Kreiger-Dougherty equation (*B*).

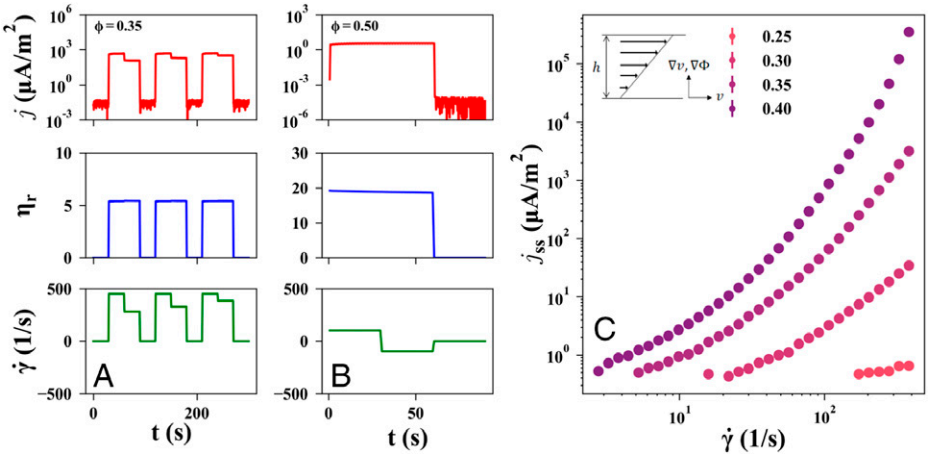

Fig. 2. (*A* and *B*) Transient current density j (*Top*), reduced viscosity η_r (*Middle*), and $\dot{\gamma}$ (*Bottom*) versus time subjected to (*A*) a sequence of step-up and step-down shear rate tests with a 30-s hold at 0 1/s ($\phi = 0.35$) and (*B*) flow reversal tests where the flow is initiated in the forward direction at 100 1/s for 30 s and then instantaneously reversed for 30 s at the same shear rate in the opposite direction before returning to the 0 1/s for 30 s. (*C*) The steady-state current density j_{ss} versus shear rate for each volume fraction tested. Note measurements below the resolution of the source meter are not shown. The inset shows that the electric field is applied along the flow gradient direction for parallel plate geometry separated by gap h.

time decreased with decreasing shear rate at fixed volume fraction and decreased with increasing volume fraction as well. These measured results qualitatively agreed with the change in current densities, which increased with increasing shear rate and volume fraction (Fig. 2*C*).

To further access relaxation rates outside the limitations of the chronoamperometry measurements, IS was used. The frequency dependence of IS measurements probes electrical and dipolar relaxation processes. We carried out these measurements on suspensions within a custom-built Couette dielectric geometry that permits frequency-dependent measurements under transient and steady shear flows (20, 21). For these measurements, raw impedance data were collected under steady shear conditions and corrected for the stray inductance and resistance of the geometry at each frequency. The resulting complex impedance Z^* was then used to calculate the complex admittance, whose real component is the alternating current (AC) conductivity σ. We found that AC conductivity was reproducible for each condition tested, and σ showed a large increase in magnitude with increasing shear rate as in our direct current (DC) electrical measurements. We also observed a low-frequency terminal regime characterized by a frequency-independent σ that transitioned to a high-frequency regime where $\sigma \sim f^p$, with f as the applied frequency and p as any value between 1 and 2.

These characteristics are commonly observed in disordered conducting systems (22–24). For shear rates and volume fractions where the terminal regime was present, we determined

$$\sigma_0 = lim_{\omega \to 0}\sigma \quad [5]$$

and fitted

$$\sigma = \sigma_0 \frac{i\tilde{\omega}}{ln(1 + i\tilde{\omega})}, \quad [6]$$

which describes the dielectric response of time-continuous random walk (25). In this expression, $\tilde{\omega} = \omega/\omega_c$ is an electrical Deborah number, where ω_c is the characteristic rate of a charge as it transits over the largest barrier associated with the DC conductivity. We interpret this time scale as dividing intracluster from intercluster transport, and it is therefore related to the transport on microscopic length scales. The observed $\tilde{\sigma} = \sigma/\sigma_0$ for each volume fraction and shear rate (summarized in Fig. 4*A*)

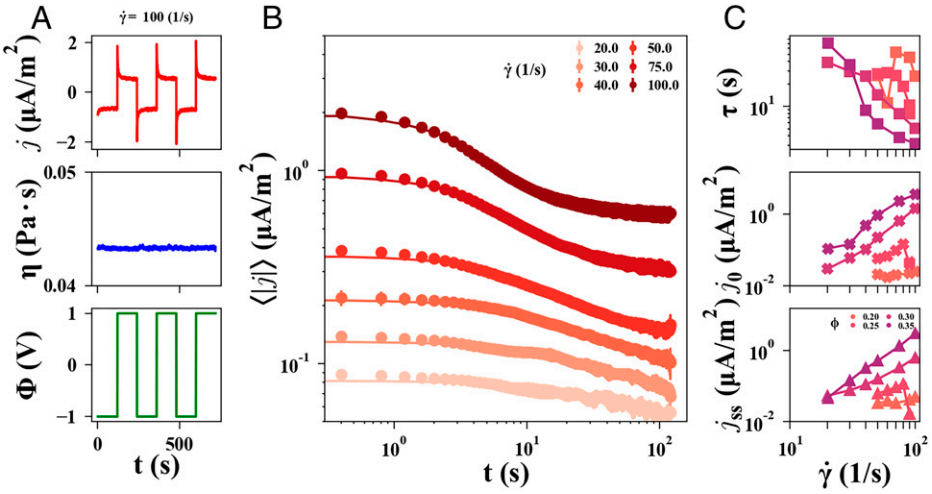

Fig. 3. Chronoamperometry of a $\phi = 0.30$ suspension. (*A*) Transient current density j (*Top*), viscosity η (*Middle*), and potential Φ (*Bottom*) for a $\dot{\gamma} = 100\ 1/s$. (*B*) Mean transient current averaged over six pulses as a function of shear rate (specified in the legend). (*C*) Results of fitting of average current relaxation curve to [4], including the measured relaxation rate τ (*Top*), the initial current density (*Middle*), and the steady-state current density (*Bottom*) for each volume fraction (0.20, 0.25, 0.30, 0.35).

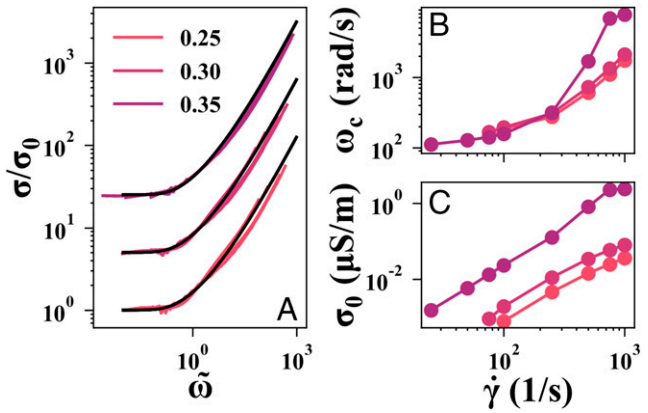

Fig. 4. (*A*) The normalized conductivity σ/σ_0 plotted versus the dimensionless frequency ω/f_e as a function of shear rate and volume fraction in Couette dielectric geometry. For each volume fraction, the curves are offset by a multiplicative factor of 5. (*B*) ω_c and (*C*) σ_0 versus $\dot{\gamma}$ for each volume fraction determined from fits to [6].

were overlaid with the model equation offset for each volume fraction by a factor of 5. There was excellent agreement with the model's functional form, and the AC conductivity appeared to obey universality that is ubiquitous in disordered systems (22, 23, 26). There were modest deviations at higher frequencies that arose due to a presence of a dielectric loss peak (*SI Appendix*, Fig. S2). Both ω_c and σ increased with increasing shear and volume fraction in Fig. 4*B* and *C*, consistent with our DC electrical measurements. The presence of a dielectric loss feature was associated with the polarization of charge carriers over a conductive cluster (27). While this polarization process was associated with the DC transport, it appeared at frequencies higher than ω_c, indicating the polarization with a conductive cluster was fast with respect to the delocalization of charge between conductive clusters (*SI Appendix*, Figs. S4 and S8).

To comprehensively understand the rheo-electrical response, we summarize the experimental results of DC and AC electrical measurements in Fig. 5*A*–*D*. In general, both transient current and IS measurement exhibited electrical relaxation that increases in its rate with increasing shear rate and volume fraction, which suggests that the transport process is dependent upon the particle self-diffusion. To describe it, we adopted a semiempirical scaling expression, $D \sim \phi\dot{\gamma}a^2 g(\phi)$, where $g(\phi) = 1/S_{Q\to 0}(\phi)$ and $S_{Q\to 0}(\phi)$ is the zero wave-vector static structure factor for a dense suspension in equilibrium, given by the Carnahan-Starling approximation (28). This expression has been used by Leshansky et al. (29) to modify the dilute limit collision frequency $\phi\dot{\gamma}$ for dense suspensions and has been shown to be accurate up to modest volume fractions $\phi \sim 0.30$. Using this relatively simple scaling law, the macroscopic relaxation time τ, measured using chronoamperometry, and the microscopic transport rate ω_c, measured using IS versus $\phi\dot{\gamma}a^2 g(\phi)$, are plotted in Fig. 5*A* and *B*, respectively. We observed the collapse of the experimental data across all volume fractions, indicating that this form accurately captures the volume fraction scaling of the transport rate. We did the same (Fig. 5*C*) for the specific conductivity σ/ϕ for both AC and DC conductivity measurements at $\Phi = 0.1$ V, and the collapse of the experimental data were observed again. Finally, we could compare the magnitudes of the macroscopic and microscopic transport rates that emerged directly from chronoamperometry and IS experiments by calculating the charge carrier diffusivity D_c. Here, D_c is given as $h^2/4\tau$ for the chronoamperometry experiments, where $h/2$ is the half-gap spacing of the symmetric rheo-electric geometry; and we used $D_c = a^2\omega_c$ for the IS measurements, where a is the mean particle radius. The result of this transformation is shown in Fig. 5*D* versus $\phi\dot{\gamma}a^2 g^{\infty}(\phi)$. We found that the scaling law not only collapsed both time scales at all volume fractions and shear rates, but also quantitatively predicted the observed diffusivities using the relationship $D_c = 0.5\phi\dot{\gamma}a^2 g^{\infty}(\phi)$, as shown by the solid line with no adjustable parameters. These results confirmed that the electrical response was governed by the charge transport process that was dependent on the particle self-diffusion. It is also interesting that the electrical transport process between particles allowed for the direct interrogation of the microscopic dynamics of the suspended particles in shear flow.

The collapse of the specific conductivity indicated that the electrons transport via a diffusive process with a rate set by D_c, a property that emerged from the dynamics of the particle motion induced by the shear flow. Diffusive transport is described by the Einstein diffusion equation $\sigma/\phi = \frac{e^2}{V_p kT} D_c\langle z^2\rangle$, where $\langle z^2\rangle$ is the mean-squared valence of the charge on each particle. This form is similar to the transport described by Eicke et al. to describe migration in dilute solutions of inverse emulsions undergoing Brownian motion (30). However, the distinction here is that the particles themselves are not the charge carriers; instead, the electrons delocalize on a time scale determined by the particle self-diffusion. It should be noted that for dilute non-Brownian suspensions, the pair-trajectories of particles are fully reversible and produce no net particle diffusion in the shear gradient direction (the direction along which our electrical measurements are made). This symmetry could be broken when multibody interactions were considered. As Acrivos has shown, three or more interacting spheres could lead to a lateral displacement of particles in the shear-gradient direction (31, 32). The three-body interactions would yield a gradient diffusivity proportional to $\phi^2\dot{\gamma}a^2$. Instead of gradient diffusion of the particles, we hypothesize that the role of shear flow is to bring the particles within a distance where electron hopping is likely to occur. The exchange of electrons during these near-field interactions produces a polarization of the electron-hole pair across pairs or clusters

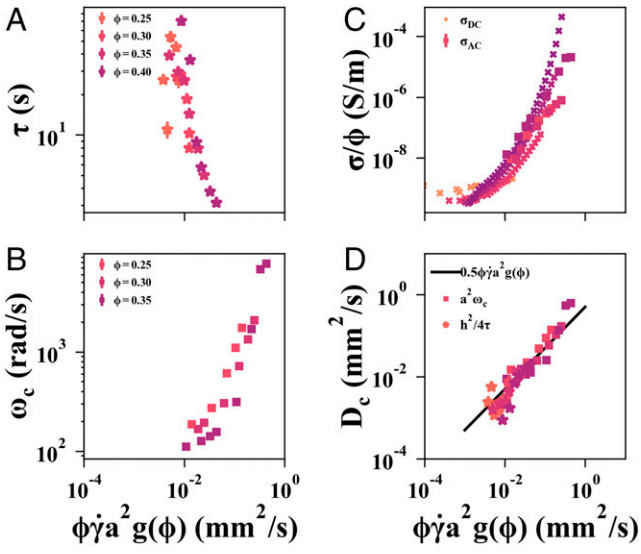

Fig. 5. (*A*–*D*) Summary of the electrical measurements versus the scaling parameter $\phi\dot{\gamma}a^2 g(\phi)$ for ϕ (0.25, 0.30, 0.35, 0.40), (*A*) current relaxation time τ, (*B*) microscopic transport rate ω_c, (*C*) specific conductivity σ/ϕ calculated from the DC measurements for ϕ (0.25, 0.30, 0.35, 0.40) and AC measurements for ϕ, and (*D*) D_c calculated using $a^2\omega_c$ and $h^2/4\tau$ for all volume fractions and shear rates. The black solid line is $0.5\phi\dot{\gamma}a^2 g(\phi)$. The colors of the symbols correspond with the volume fraction.

of particles that could become delocalized if the shear is sufficiently fast. Therefore, the rate of electrical transport is dependent upon the time scale of microstructure rearrangement, as well as on the ability of charges to delocalize over distances that exceed the particles themselves along the gradient direction. This is distinct and distinguishable from the process where the charge carriers remain strongly bound to the particles and transport through the gradient diffusion of the particles alone.

To test this hypothesis, we employed large-scale Stokesian dynamics simulations coupled with a kinetic Monte Carlo–based approach to compute charge transport within sheared non-Brownian suspensions. We used a recently developed Stokesian dynamic simulation tool that accurately and rapidly computes the microstructure under flow while including the hydrodynamic interactions between particles (33). To validate the simulations, suspension shear viscosities, mean-squared displacements (MSDs), and gradient diffusivities $\tilde{D}_p^y$ were calculated as a function of ϕ (0.25, 0.30, 0.35), and we found that their values compared quantitatively with our experimental results as well as to the results of Stokesian dynamics simulations (*SI Appendix*, Fig. S3) (34). To simulate the electrical transport process across the computed suspension microstructures, we employed a kinetic Monte Carlo scheme and developed a two-parameter model to estimate gradient charge diffusivities $\tilde{D}_c^y$ as a function of suspension concentration. Using this two-parameter model, we calculated the MSD of the charges and the $\tilde{D}_c^y$ and explored the effect of δ and k_0 on $\tilde{D}_c^y$ (*SI Appendix*, Figs. S5 and S7). Note that assuming an instant delocalization of charges within a conductive cluster instead of a finite charge transfer rate leads to a simpler model with one parameter δ, which predicts a D_{yy} that matches with experiments for $\phi = 0.25$ suspension when $\delta = 0.015$ but overpredicts for higher concentrations.

We found quantitative agreement with the experiments over the entire volume fraction tested when $\delta/a = 0.001$ and $k_0\Delta t = 0.6$ (Fig. 6*A*). To match simulations, it is necessary to define a dimensionless gradient diffusivity according to $\tilde{D}_c^y = D_c/(4\dot{\gamma}a^2)$, where the factor of 4 is determined empirically. The simulations provide a quantitative prediction of the measured $\tilde{D}_c^y$, and the solid black line gives the prediction that $\tilde{D}_c^y = \phi g_0(\phi)/8$, where the factor of 8 is determined empirically. These charge diffusivities could be compared with the particle diffusivities based on the prediction given by Acrivos that $\tilde{D}_p^y = \phi^2/2$, which showed good agreement with both our simulation results and the measurements by Leighton (31). These results demonstrated that not only does the charge transport model based on the kinetic Monte Carlo scheme described here quantitatively match our experimental results, but also that electrical transport cannot be explained through the gradient diffusivity of the particles alone. The gradient diffusion induced by flow is an order of magnitude slower than the self-diffusion expression proposed here. This distinction could be understood when we examine the probability density functions (PDFs) of the particle (Fig. 6*B*) and charge (Fig. 6*C*) displacements $\Delta\tilde{y}$ along the gradient direction extracted from our simulations. The PDF plots showed that the particle displacements were as large as $\Delta y = 0.1a$. With increasing ϕ, the PDF broadened, and larger Δy became more probable, resulting in the increase of particle self-diffusivity. However, the PDFs of the charge displacements appeared qualitative and quantitatively different. First, the frequencies of small displacements ($\Delta y < 2a$) were larger and more probable for the charges than for the particles. This enhancement was associated with the exchange of charges between pairs of particles. For large displacements ($\Delta y > 2a$), the charges are delocalized over dynamic clusters that orient in the compressional direction of shear. Note that the PDF of these large charge displacements followed the same trend as the PDF of the cluster sizes in gradient direction for $\Delta y > 2a$

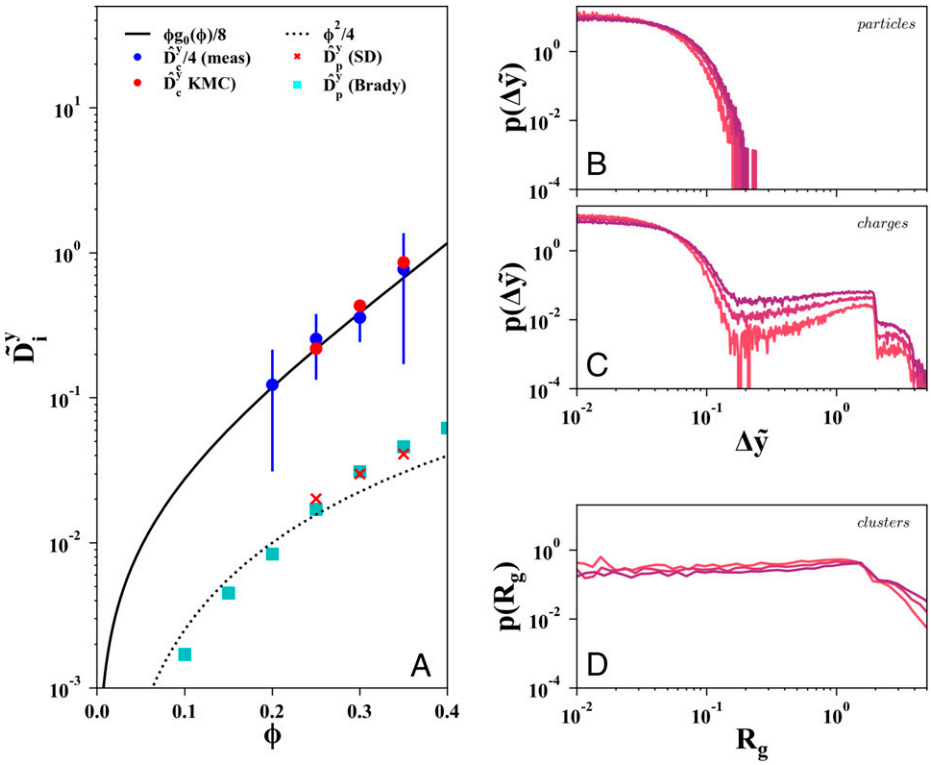

Fig. 6. (*A*) Comparison of the measured, simulated, and predicted gradient diffusivities $\tilde{D}_i^y$ for the particles (i = p) and the charges (i = c). (*B* and *C*) The PDF of a displacement of magnitude $\Delta\tilde{y}$ for the (*B*) particles and (*C*) charges for ϕ (0.25, 0.30, 0.35). (*D*) PDF of cluster size in gradient direction y_c.

(Fig. 6*C* and *D*), indicating that the large charge displacements were due to charge delocalization across clusters. The combination of large displacements along the compressional direction, along with more frequent hopping events, leads to higher diffusivity values for the charges as compared to the particles. The physical connection between particles and cluster formation upon shearing is also studied by the simulation. The size of conductive clusters increases with increases of both suspension concentration (ϕ) and the charge hopping length scale (δ/a),—as the microstructure images show in *SI Appendix*, Fig. S6—and the normalized probability distribution of cluster lengths along the gradient direction (*SI Appendix*, Fig. S9).

In summary, we use both experimental and simulation methods to study electron transport in suspensions of non-Brownian silver microspheres. We used transient DC and AC electrical techniques to determine the electrical diffusivity and adopted a semiempirical scaling expression that quantitatively predicts the rate of the hopping process. We compared the measured diffusivities to those determined using accurate large-scale Stokesian dynamic simulations coupled with a Monte Carlo–based method to represent the charge transport. Comparing the experiments and simulations, we found quantitative agreement and used the simulations to demonstrate that the electrical diffusivity is faster than the particle gradient diffusion, confirming that transport is mediated by the delocalization of electrons across dynamic clusters that form in shear flow.

Materials and Methods

Materials. Hollow glass microspheres (Cospheric-HGMS-AG) were purchased and found to have a particle diameter $a = 5$ to 15 μm and a reported density $\rho_p = 1.08$ g/mL. These particles have a thin shell of silver metal, $t_{shell} = 100$ nm. The particles are suspended in silicone oil, AR200 (Aldrich), $\rho_s = 1.05$ g/mL and $\eta_s = 200\ mPa \cdot s$. Suspensions were prepared based on the dry mass volume fraction ϕ. For each batch of particles, we observed minor differences in the observed current density that we believe originates from variation in batch-to-batch coating density of the silver-coated microspheres. While the current densities were reproducible within a given batch, comparing across batches showed, in some cases, minor inconsistencies. This results in the spread of the observed conductivities in Fig. 5*C*. Within a given batch of particles, field-dependent measurements show Ohmic behavior. Before measurement, the suspensions were vortexed for 2 h, roll-mixed overnight, and degassed at room temperature. These suspensions remain stable for several hours but show the evidence of aggregation and sedimentation overnight. Therefore, they are freshly prepared prior to each measurement.

Experimental Methods. Rheo-electric measurements were performed using an ARES G2 strain-controlled rheometer (TA Instruments) with a 25-mm parallel plate accessory modified to enable electrical measurements under steady and transient shear experiments (20, 21, 35). All measurements were performed using 0.5-mm gap. DC conductivity measurements were performed with a Keithley 2450 source meter with an applied voltage of 0.1 V unless otherwise stated. The steady-state current was measured at each shear rate, averaged, and used to compute the conductivity with the known cell constant of 6.4 m calibrated using salt solutions of known conductivity. For transient testing, the samples were subjected to steady shear, and the voltage varied from 1 to −1 V in 120-s intervals. This was repeated six times, and the resulting absolute value of the current density was averaged for each pulse to produce the current relaxation. These data were further filtered using a bandpass filter to remove high-frequency noise. Impedance measurements were made with a Keysight 4980A LCR Meter in a two-electrode configuration with a 50-mV voltage amplitude using a Couette rheo-electric device with a cell constant of 6.7 m. The complex impedance was corrected for the stray impedance and inductance of the cell using open and short circuit measurements. At each frequency, the complex impedance was converted to the admittance $Y^* = 1/Z^* = \sigma - j(2\pi\varepsilon_0\varepsilon')$, where ε_0 is the permittivity of free space (36).

Simulation Methods. A recently developed Stokesian dynamics simulation tool is used to compute the microstructure evolution of a sheared non-Brownian suspension (33, 37). Long-ranged hydrodynamic interactions were modeled using the Rotne-Prager-Yamakawa tensor (38, 39), and the lubrication interactions were modeled using exact expressions proposed by Jeffrey and Onishi (40, 41). Our simulations were performed with 2,197 monodisperse particles of unit radii ($a = 1$) in a cubic simulation box of different sizes corresponding to the three particle volume fractions $\phi = 0.25$, 0.30, and 0.35. Particles are suspended in a solvent with viscosity $\eta = 1/6\pi$. A unit shear rate ($\dot{\gamma} = 1$) is applied in the gradient (y) direction of the shear flow using Lees-Edwards boundary conditions. Periodic boundary conditions are applied in the flow and vorticity (x, z) directions. A pairwise repulsive force $F = F_0\tau_R e^{-\tau_R h}/(1 - e^{-\tau_R h})$ is employed to keep particles from overlapping, where h is the minimum surface separation between the particles, and F_0 and τ_R are the magnitude and range of the interparticle force, respectively. We chose $F_0\tau_R = 1$ and $\tau_R = 1000$, similar to Sierou and Brady in their simulations of sheared non-Brownian suspensions (34).

A kinetic Monte Carlo–based approach is used to compute the charge transport across the computed suspension microstructures. We developed a model to compute the charge diffusivity in gradient direction D_c^y as a function of suspension concentration. In this model, the charge hopping between the surfaces of two neighboring particles in a flowing suspension occurs only when the minimum surface separation between the particles is less than a critical length scale δ, and the charge hopping occurs at a finite rate k_0. The particle microstructures at regular time intervals (Δt) are obtained from the Stokesian dynamics simulations. A number of charges are seeded onto the particles randomly across the initial microstructure. The clusters for charge hopping are identified such that the minimum surface separation between any two neighboring particles within the cluster is less than δ/a. Charges in each cluster hop to their neighboring particles of the same cluster, and the number of hopping steps during a simulation time step is $k_0\Delta t$, where k_0 is hopping rate, the second parameter of the Kinetic Monte Carlo (KMC) model. For larger values of k_0, the charges can transport to longer distances in the cluster within the simulation time step, which results in higher overall charge diffusivities. The final locations of the charges at the end of the simulation time step are then transferred to the corresponding particles in the second microstructure, and the charge transport computation is repeated. This procedure is continued for all the microstructures within 100 strain units of steady state, and the time evolution of charge positions is recorded, which is used to compute the mean square displacements of charges and their gradient diffusivities (D_c^y). The dependence of charge hopping on the applied field is ignored in this model. The complex charge transport processes between particles of flowing suspension are lumped into this simple coarse-grained KMC model with two parameters whose predictions match well with the experiments.

Data Availability. All study data are included in the article and/or supporting information.

ACKNOWLEDGMENTS. The rheo-electric measurements benefited from funding support from the National Science Foundation (CBET-2047365). H.L. was partially funded by the Department of Energy Basic Energy Science Program (#DE-SC0022119) and by Leslie and Mac McQuown through the Center for Engineering Sustainability and Resilience at Northwestern. We also would like to acknowledge the contribution of Matt Snell for his preliminary measurements on this project. M.V.M. was partially funded by the Skoltech - MIT Next Generation Program during this work.

1. U. Genz, J. A. Helsen, J. Mewis, Dielectric spectroscopy of reversibly flocculated dispersions during flow. *J. Colloid Interface Sci.* **165**, 212–220 (1994).
2. J. Mewis, L. M. De Groot, J. A. Helsen, Dielectric behavior of flowing thixotropic suspensions. *Colloids Surf.* **22**, 249–269 (1987).
3. M. Youssry, D. Guyomard, B. Lestriez, Suspensions of carbon nanofibers in organic medium: Rheo-electrical properties. *Phys. Chem. Chem. Phys.* **17**, 32316–32327 (2015).
4. M. Youssry *et al.*, Formulation of flowable anolyte for redox flow batteries: Rheo-electrical study. *J. Power Sources* **274**, 424–431 (2015).
5. L. Madec *et al.*, Electronic vs. ionic limitations to electrochemical performance in Li 4 Ti 5 O 12 -based organic suspensions for lithium-redox flow batteries. *J. Electrochem. Soc.* **161**, A693–A699 (2014).
6. A. Helal, T. Divoux, G. H. McKinley, Simultaneous rheoelectric measurements of strongly conductive complex fluids. *Phys. Rev. Appl.* **6**, 64004 (2016).

7. M. Youssry *et al.*, Non-aqueous carbon black suspensions for lithium-based redox flow batteries: Rheology and simultaneous rheo-electrical behavior. *Phys. Chem. Chem. Phys.* **15**, 14476–14486 (2013).
8. A. Narayanan, F. Mugele, M. H. G. Duits, Mechanical history dependence in carbon black suspensions for flow batteries: A rheo-impedance study. *Langmuir* **33**, 1629–1638 (2017).
9. A. Narayanan, F. Mugele, M. H. G. Duits, Device for rheometry, impedance spectroscopy, and electrochemistry on fluid electrodes. *Rev. Sci. Instrum.* **90**, 025112 (2019).
10. A. Narayanan *et al.*, Influence of electrochemical cycling on the rheo-impedance of anolytes for Li-based semi solid flow batteries. *Electrochim. Acta* **251**, 388–395 (2017).
11. J. B. Hipp, J. J. Richards, N. J. Wagner, Direct measurements of the microstructural origin of shear-thinning in carbon black suspensions. *J. Rheol. (N.Y.N.Y.)* **65**, 145–157 (2021).
12. J. B. Hipp, J. J. Richards, N. J. Wagner, Structure-property relationships of sheared carbon black suspensions determined by simultaneous rheological and neutron scattering measurements. *J. Rheol. (N.Y.N.Y.)* **63**, 423–436 (2019).
13. J. J. Richards, J. B. Hipp, J. K. Riley, N. J. Wagner, P. D. Butler, Clustering and percolation in suspensions of carbon black. *Langmuir* **33**, 12260–12266 (2017).
14. D. Quemada, Rheology of concentrated disperse systems and minimum energy dissipation principle. *Rheol. Acta* **16**, 82–94 (1977).
15. D. Quemada, An overview of recent results on rheology of concentrated colloidal dispersions. *Trends Colloid Interface Sci.* **III**, 112–119 (1989).
16. M. M. Denn, J. F. Morris, Rheology of non-Brownian suspensions. *Annu. Rev. Chem. Biomol. Eng.* **5**, 203–228 (2014).
17. M. Parthasarathy, D. J. Klingenberg, Electrorheology: Mechanisms and models. *Mater. Sci. Eng. Rep.* **17**, 57–103 (1996).
18. A. Acrivos, X. Fan, R. Mauri, On the measurement of the relative viscosity of suspensions. *J. Rheol. (N.Y.N.Y.)* **38**, 1285–1296 (1994).
19. P. Stallinga, H. L. Gomes, Thin-film field-effect transistors: The effects of traps on the bias and temperature dependence of field-effect mobility, including the Meyer–Neldel rule. *Org. Electron.* **7**, 592–599 (2006).
20. J. J. Richards, C. V. L. Gagnon, J. R. Krzywon, N. J. Wagner, P. D. Butler, Dielectric RheoSANS–Si1multaneous interrogation of impedance, rheology and small angle neutron scattering of complex fluids. *J. Vis. Exp.* **122**, 55318 (2017).
21. J. J. Richards, N. J. Wagner, P. D. Butler, A strain-controlled RheoSANS instrument for the measurement of the microstructural, electrical, and mechanical properties of soft materials. *Rev. Sci. Instrum.* **88**, 105115 (2017).
22. G. A. Niklasson, Comparison of dielectric response functions for conducting materials. *J. Appl. Phys.* **66**, 4350–4359 (1989).
23. A. K. Jonscher, Electronic properties of amorphous dielectric films. *Thin Solid Films* **1**, 213–234 (1967).
24. K. Weron, How to obtain the universal response law in the Jonscher screened hopping model for dielectric relaxation. *J. Phys. Condens. Matter* **3**, 221 (1991).
25. J. C. Dyre, Unified formalism for excess current noise in random-walk models. *Phys. Rev. B Condens. Matter* **37**, 10143–10149 (1988).
26. G. A. Niklasson, Fractal aspects of the dielectric response of charge carriers in disordered materials. *J. Appl. Phys.* **62**, R1–R14 (1987).
27. R. Pelster, U. Simon, Nanodispersions of conducting particles: Preparation, microstructure and dielectric properties. *Colloid Polym. Sci.* **277**, 2–14 (1999).
28. N. F. Carnahan, K. E. Starling, Equation of state for nonattracting rigid spheres. *J. Chem. Phys.* **51**, 635–636 (1969).
29. A. M. Leshansky, J. F. Morris, J. F. Brady, Collective diffusion in sheared colloidal suspensions. *J. Fluid Mech.* **597**, 305–341 (2008).
30. H. F. Eicke, M. Borkovec, B. Das-Gupta, Conductivity of water-in-oil microemulsions: A quantitative charge fluctuation model. *J. Phys. Chem.* **93**, 314–317 (1989).
31. D. Leighton, A. Acrivos, Measurement of shear-induced self-diffusion in concentrated suspensions of spheres. *J. Fluid Mech.* **177**, 109–131 (1987).
32. A. Acrivos, BINGHAM AWARD LECTURE–1994 Shear-induced particle diffusion in concentrated suspensions of noncolloidal particles. *J. Rheol. (N.Y.N.Y.)* **39**, 813–826 (1995).
33. J. W. Swan, G. Wang, Rapid calculation of hydrodynamic and transport properties in concentrated solutions of colloidal particles and macromolecules. *Phys. Fluids* **28**, 011902 (2016).
34. A. Sierou, J. F. Brady, Rheology and microstructure in concentrated noncolloidal suspensions. *J. Rheol. (N.Y.N.Y.)* **46**, 1031–1056 (2002).
35. J. J. Richards, J. K. Riley, Dielectric RheoSANS: A mutual electrical and rheological characterization technique using small-angle neutron scattering. *Curr. Opin. Colloid Interface Sci.* **42**, 110–120 (2019).
36. E. Barsoukov, J. R. Macdonald, *Impedance Spectroscopy Theory, Experiment, and Applications* (John Wiley &Sons, Inc., Hoboken, NJ, ed. 2, 2005).
37. A. M. Fiore, J. W. Swan, Fast Stokesian dynamics. *J. Fluid Mech.* **878**, 544–597 (2019).
38. H. Yamakawa, Transport properties of polymer chains in dilute solution: Hydrodynamic interaction. *J. Chem. Phys.* **53**, 436–443 (1970).
39. J. Rotne, S. Prager, Variational treatment of hydrodynamic interaction in polymers. *J. Chem. Phys.* **50**, 4831–4837 (1969).
40. D. J. Jeffrey, Y. Onishi, Calculation of the resistance and mobility functions for two unequal rigid spheres in low-Reynolds-number flow. *J. Fluid Mech.* **139**, 261–290 (1984).
41. D. J. Jeffrey, The calculation of the low Reynolds number resistance functions for two unequal spheres. *Phys. Fluids A Fluid Dyn.* **4**, 16–29 (1992).